Selectively Absorbing Small-Molecule Solar Cells for Self-Powered Electrochromic Windows

# Selectively Absorbing Small-Molecule Solar Cells for Self-Powered Electrochromic Windows

Xiangkun Jia[1,#], Elizabeth Christine Baird[1,#], Jan Blochwitz-Nimoth[1], Sebastian Reineke[1,*], Koen Vandewal[2,*], Donato Spoltore[1,*]

[1] *Dresden Integrated Center for Applied Physics and Photonic Materials (IAPP) and Institute for Applied Physics, Technische Universität Dresden, Nöthnitzer Str. 61, 01187 Dresden, Germany*

[2] *Institute for Materials Research (IMO-IMOMEC), Hasselt University, Wetenschapspark 1, 3590 Diepenbeek, Belgium*

[#] These authors contributed equally: Xiangkun Jia, Elizabeth Christine Baird

[*] Corresponding authors

E-mail addresses: (sebastian.reineke@tu-dresden.de, koen.vandewal@uhasselt.be, donato.spoltore@tu-dresden.de)

**Abstract**

Dynamic control of solar transmission by photovoltaic-powered electrochromic smart windows is an up-and-coming approach towards the reduction of energy consumption in buildings. Selectively-absorbing transparent organic solar cells are capable of exhibiting excellent visible-light transparency as well as respectable power conversion efficiencies. This work presents three different transparent small-molecule solar cells (TSCs) with an area of 2.52 $cm^2$, two of which are UV-absorbing and one of which absorbs in the NIR, each in combination with an organic electrochromic device (EC). The NIR-absorbing TSC uses a BDP-OMe:$C_{60}$ combination, and has a power conversion efficiency of 4% with an average visible light transmission (AVT) of 40%. The two UV-harvesting systems, α-6T/B4PYMPM and NPB:B4PYMPM, each have an AVT of 50-65%, as well as high open-circuit voltages of 1.5-2.0 V. We demonstrate that these photogenerated voltages are sufficient to power a fluoran dye-based organic EC, which has excellent optical properties: its color ranges from highly transparent to deep black, and its on/off contrast ratio is higher than 80% in the range between 390 nm and 640 nm. Self-powered smart windows made by the combination of TSCs and ECs provide a way to significantly reduce energy consumption from air conditioning and lighting, towards zero-energy buildings.

**Keywords:** small-molecules; solar cells; electrochromic devices; smart windows; self-sustainable

## 1. Introduction

Heating, air conditioning, and lighting in buildings account for a major portion of electricity demand, around 40% of overall energy usage as of 2018 [1]. With the effects of climate change rapidly worsening, it is imperative that we find ways to reduce this energy burden. Adaptation of PV technology into building-integrated photovoltaics (BIPV), which act as self-powering temperature-regulating building envelopes, could help to alleviate this issue in different ways [2,3]. BIPV can minimize long-distance transmission losses and installation costs by generating electricity close to where it is utilized, for example on roofs, facades, and solar shading systems [4]. One especially promising branch of BIPV involves electrochromic smart windows powered by transparent photovoltaic modules. These self-sufficient devices regulate the transmission of solar radiation through building windows, controlling the interior climate without increasing energy usage [5–7]. By reducing the amount of electricity required to manage indoor temperature and lighting, these devices can help to mitigate the overall energy consumption, thereby contributing to fight climate change. In this paper, we will present a BIPV system consisting of a combination of an electrochromic device (EC) and transparent solar cells (TSCs), each of which can be easily fabricated from organic materials.

In order to create a self-sustaining TSC-EC module, the power conversion efficiency (PCE) and average visible light transmission (AVT) of TSCs need to be balanced [8]. Transparent polymer solar cells with PCEs of 3-13% have been demonstrated in the past with AVTs in the range of ~ 10-50% [8–14]. However, when using blade coating method to increase those devices' active area over 1 $cm^2$, their fill factors, photocurrents and PCEs drop, indicating scalability problems and limited usefulness in larger applications [15–18]. The selectively absorbing small-molecule

TSCs presented here have superior AVTs and scalability potential compared to polymer-based transparent solar cells [19]. Among them, the near-infrared (NIR)-absorbing TSCs with an area of 2.52 $cm^2$ exhibit, to the best of our knowledge, the highest PCE (~ 4%) in combination with an AVT of 40%, compared to other reported small-molecule based TSCs [20–23]. While the near-ultra-violet (UV) absorbing TSCs offer photovoltages of 1.5-2.0 V, enough to control light transmission through the EC devices, the NIR devices require a series connection to achieve sufficiently high voltages. However, the larger photocurrent (~ 10 mA $cm^{-2}$) achieved by the NIR TSCs in comparison with that of near-UV TSCs partially compensates for their lack of photovoltage. The UV-absorbing TSCs have outstanding AVTs of up to 65%, along with excellent solar heat gain coefficient (SHGC) values reaching 60%. The SHGC values indicate that these UV-absorbing TSCs are good candidates for powering EC windows in colder climates where additional heating is advantageous. On the other hand, the NIR-harvesting device would provide more benefit in hot climates, since they block some of the IR radiation to prevent the indoor from overheating.

Most commercially available electrochromic technologies operate by an electrochemical oxidation/reduction reaction between inorganic metal oxide thin films, usually tungsten and nickel oxide [24–27]. The EC system presented here diverges from this traditional configuration. Instead of metal oxides, it is based on a type of dye commonly referred to as fluoran. Fluoran dyes have been widely utilized as a component of thermal paper, and are reported as the active agent in a handful of reports on EC devices [28,29]. Fluoran-based EC systems have been studied most extensively by the Information Display group at Kyung-Hee University. They have investigated the use of fluoran EC in several applications, including as a component in

augmented reality headsets and as part of an OLED-EC combination [30,31]. However, fluoran EC has yet to be reported in smart window applications. Studies on the optical properties of this material for ECs have shown that the performance of fluoran derivatives are comparable to those of commercially available electrochromic windows, which offer a transparent-state transmittance of 65%-78% and a darkened-state transmittance of 1%-4% [32].

## 2. Experimental section

### *2.1. Sample preparation*

#### *2.1.1. Small-molecule solar cells preparation*

The layers of the small-molecule solar cells are thermally evaporated at ultra-high vacuum (base pressure < $10^{-7}$ mbar) on a glass substrate with a pre-structured ITO contact (Thin Film Devices, USA). Glass substrates are cleaned in a multi-step wet process including rinsing with N-methyl-2-pyrrolidone, ethanol, and deionized water as well as treatment with ultraviolet ozone. The performances of the small molecule solar cells are optimized for opaque devices, before making them transparent. The optimization steps are shown in Figure S1-3 and Table S1-3. In order to make the optimized devices transparent, the thickness of the top Ag electrode is reduced from 100 to 7 nm. The structures of devices and of the used materials for all transparent solar cells are listed in Table S4. All organic materials are purified 2-3 times by sublimation. The device area is defined by the geometrical overlap of the bottom and the top contact, the active area of standard and large-area devices equals 6.44 $mm^2$ and 2.52 $cm^2$, respectively. To avoid exposure to ambient conditions, the organic part of the device is covered by a small glass substrate, which is glued on top.

104 *2.1.2. Organic electrochromic devices preparation*

105 The electrochromic solution contains chemical components in the following approximate
106 concentrations: 0.3M tetrabutylammonium tetrafluoroborate, 0.5M black fluoran dye and 0.5M
107 hydroquinone in N,N-dimethylacetamide. All chemicals are used as received from the
108 manufacturer. Devices are all made with two pieces of ITO glass and the EC thickness is
109 determined by tape spacer.

110 *2.2. Characterization techniques*

111 Current-voltage characteristics in dark and under solar illumination are measured with an SMU
112 (Keithley 2400, USA) at room temperature in ambient conditions. The cells are illuminated
113 with a spectrally mismatch corrected intensity of 100 mW $cm^{-2}$ (AM1.5g) provided by a sun
114 simulator (16 S-150 V.3 Solar Light Co., USA). The intensity is monitored with a Hamamatsu
115 S1337 silicon photodiode (calibrated by Fraunhofer ISE Freiburg, Germany).

116 $EQE_{PV}$ measurements are taken using masks to minimize edge effects and to define an exact
117 photoactive area (2.78 $mm^2$). The $EQE_{PV}$ is detected with a lock-in amplifier (Signal Recovery
118 SR 7265) under monochromatic illumination (Oriel Xe Arc-Lamp Apex Illuminator combined
119 with Cornerstone 260 1/4m monochromator, Newport, USA) using a calibrated mono-
120 crystalline silicon reference diode (Hamamatsu S1337 calibrated by Fraunhofer ISE, Germany).

121 Transmission and reflection spectra for transparent solar cells and electrochromic devices are
122 measured by Shimadzu UV-3100 and Shimadzu solid-spec 3700 spectrometers. In order to
123 measure the transmission spectra for transparent standard devices with an area of 6.44 $mm^2$, a
124 mask is used to make sure that light pass through from the transparent active layer region only.

For large-area TSCs (2.52 $cm^2$), we measure transmission and reflection spectra in the range between 300 to 2500 nm for the calculation of SHGC. In order to measure the transmission spectra of EC devices at different applied voltages, the devices are mounted inside the UV-Vis spectrometer while being wire-connected to an external power source, a Keithley 2602 SMU or a transparent solar cells. With these spectra, CRI and CIE coordinates are calculated by ColorCalculator software produced by OSRAM Sylvania, Inc. SHGC values are obtained by utilizing the equations mentioned in Note S1.

## 3. Results and discussion

### *3.1. Chemical structures and optoelectronic properties of small-molecule TSCs*

The transparent solar cells use combinations of electron-donating and electron-absorbing materials whose chemical structures, energy levels, and absorption spectra are shown in Fig. 1. The materials NPB and α-6T are utilized as electron donors. The ionization potential (IP) and electron affinity (EA) levels of the high-gap material NPB are 5.46 and 2.45 eV respectively [33], resulting in an absorption peak at around 347 nm as shown in Fig. 1c. The IP and EA of α-6T are 5.0 and 3.0 eV respectively [34], with an optical gap around 2.0 eV and a relatively broad absorption region from 330 to 550 nm (see Fig. 1c). The absorption of NPB is localized in the UV region, while α-6T also absorbs visible light. B4PYMPM works as an electron acceptor when combined with NPB or α-6T, lending to a subtle contribution to the light absorption while providing interfaces with both donor materials which efficiently dissociate excitons into free carriers [35]. For devices absorbing in the NIR, BDP-OMe is combined with $C_{60}$. As a narrow-gap (~ 1.44 eV) small-molecule material shown in Fig. 1b, BDP-OMe has a

strong absorption peak at around 800 nm, making it a satisfactory NIR photon absorber. The absorption of BDP-OMe in the visible regions is quite weak, which is beneficial to the transmission of visible light.

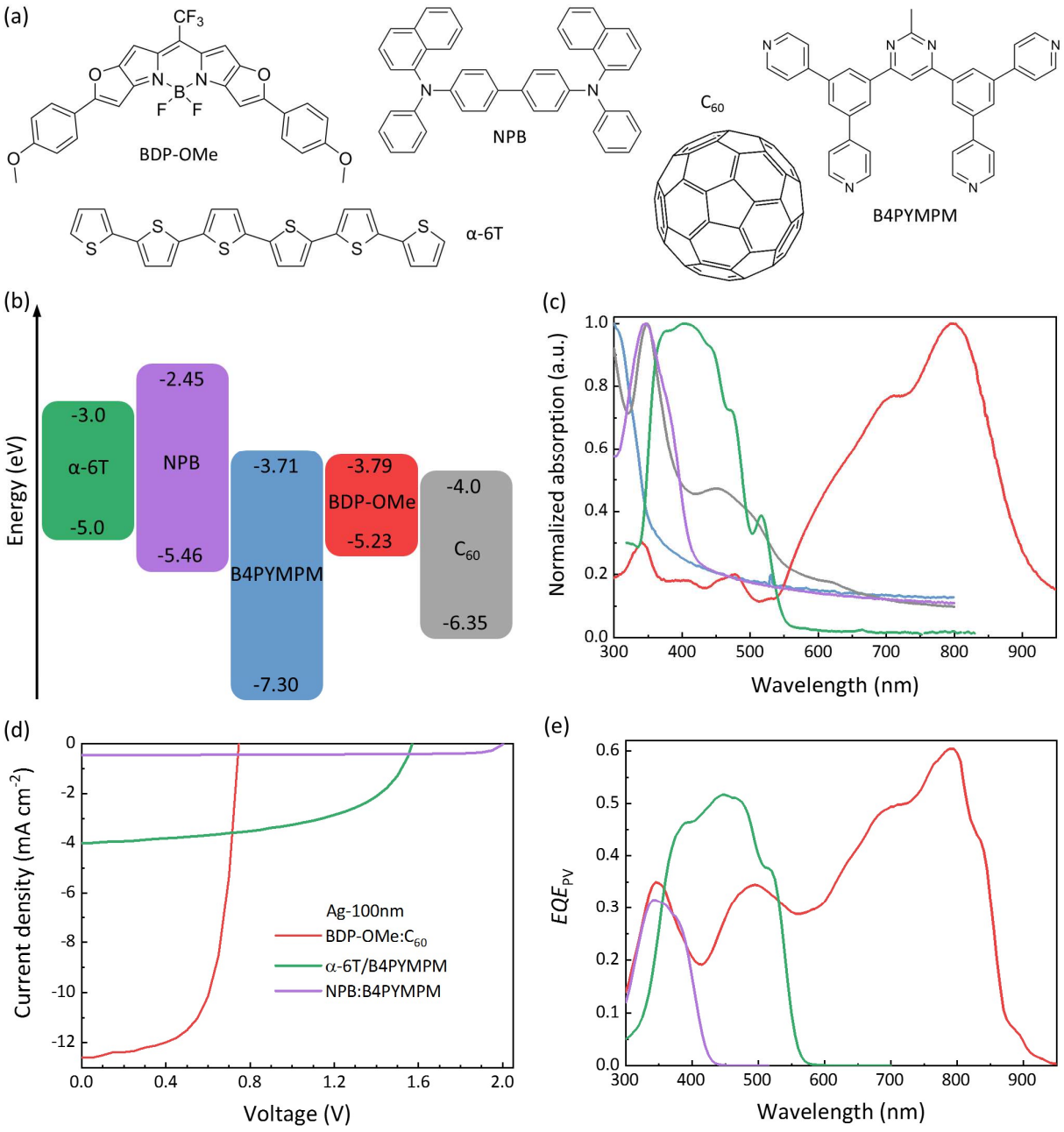


**Fig. 1.** (a) Chemical structures, (b) Energy levels, and (c) Normalized UV-Vis absorption spectra of the materials used in this work. The energy levels of α-6T [34], NPB [33], B4PYMPM [36], and $C_{60}$ [37] are obtained from the literature. (d) Current-density voltage (*J-V*) characteristics, and (e) Photovoltaic external quantum efficiency ($EQE_{PV}$) for solar cells with 100 nm thick Ag electrodes. The area of the active layer of the studied solar cells is 6.44 $mm^2$.

155 *3.2 Photovoltaic performance of TSCs*

156 Current-voltage characteristics of bulk and planar heterojunction (BHJ/PHJ) solar cells are
157 measured under simulated solar intensity (AM 1.5g). Fig. 1d-e show the photovoltaic
158 performance of 6.44 $mm^2$ opaque solar cells with 100 nm-thick Ag electrodes. The photovoltaic
159 parameters, along with the performance of devices with various thicknesses of Ag electrodes,
160 are summarized in Figure S4 and Table S5. For the near-UV light-harvesting devices, open-
161 circuit voltages ($V_{OC}$) as high as 1.57 V and 2.00 V are achieved in the planar α-6T/B4PYMPM
162 and bulk NPB:B4PYMPM junction, with fill factors (*FF*) of 54.6% and 76.3%, respectively.
163 For the α-6T devices, a higher performance is obtained for planar junction than for bulk
164 heterojunction devices (Figure S2 and Table S2). Due to its higher external quantum efficiency
165 ($EQE_{PV}$), the performance of the α-6T device is superior to that of the NPB device, with a short-
166 circuit current density ($J_{SC}$) of 4.0 mA $cm^{-2}$ and a corresponding PCE of 3.44%. When the
167 thickness of the Ag electrode is reduced to 10 nm, to make the device transparent, the PCE of
168 α-6T/B4PYMPM and NPB:B4PYMPM decreases to 1.21% and 0.44%, respectively. This is
169 mainly due to the diminished $J_{SC}$ from reduced absorption in the active layers, resulting from
170 the curtailed back reflection from the Ag top electrode. Interestingly, the $V_{OC}$ of the device with
171 the reduced-thickness Ag electrode remains unaffected. For the BHJ NIR-absorbing solar cell,
172 BDP-OMe:$C_{60}$ has a dramatically enhanced $J_{SC}$ of 12.58 mA $cm^{-2}$, which is consistent with both
173 its broad and high $EQE_{PV}$ and the fact that the sunlight provides more photons in the spectral
174 region where this device has the strongest absorption. The PCE of this BDP-OMe containing
175 device reaches 6.10%, with a *FF* of 64.9% and a $V_{OC}$ of 0.75 V. When the thickness of the Ag
176 electrode is reduced to 10 nm, the maximum $EQE_{PV}$ drops to 48%, with a corresponding drop

177 in $J_{SC}$ and PCE to 8.98 mA cm$^{-2}$ and 3.97%. However, the values for $V_{OC}$ and *FF* remain nearly
178 unchanged. The stability of those devices is also very important. Recent reports confirmed that
179 organic solar cells have operation times of several years [38], in particular thermally evaporated
180 devices exhibit enhanced stability compared to their solution-processed competitor [39].

181 *3.3 Scalability of NIR/UV-absorbing TSCs*

182 In order to demonstrate the scalability of the vacuum deposition technique used for these TSCs,
183 devices with active areas above one square centimeter are fabricated. Fig. 2 shows the
184 photovoltaic characteristics as well as the transmission and reflection spectra of these enlarged
185 devices. The performance of BDP-OMe:$C_{60}$ device drops by around 10% when the active area
186 is raised from 6.44 mm$^2$ to 2.52 cm$^2$. This is mainly due to the slightly-lowered $V_{OC}$ and *FF*,
187 the latter of which may result from the increased resistance of the larger ITO electrode [40].
188 However, this effect is nearly absent in the α-6T/B4PYMPM devices. The PCE of large-area α-
189 6T-based opaque devices reaches 3.38 %, with a $V_{OC}$ of 1.56 V, $J_{SC}$ of 3.95 mA cm$^{-2}$, and *FF* of
190 54.9%, similar to the photovoltaic parameters of the small-area device. The $V_{OC}$ and *FF* of the
191 NPB:B4PYMPM system remain unchanged when scaling up the device area to 2.52 cm$^2$, but
192 the $J_{SC}$ decreases from 0.46 to 0.27 mA cm$^{-2}$, resulting in a PCE that is diminished to 0.42%.

193 When the thicknesses of Ag electrodes are minimized to achieve transparent devices, the
194 photovoltaic performance of TSCs is reduced mainly because of a loss of back reflection and
195 an increased sheet resistance of the Ag film [41]. Nevertheless, the efficiencies of both the BDP-
196 OMe- and α-6T-based devices remain adequate even with 10 nm-thick Ag electrodes: 3.86%
197 for BDP-OMe and 1.75% for α-6T. To the best of our knowledge, the *FF* of the

NPB:B4PYMPM system presented here, which reaches up to 77.7% in a device with an active area of 2.52 $cm^2$ and a 10 nm thick Ag film, is the highest value among reported transparent small-molecule solar cells [20,21,42,43].

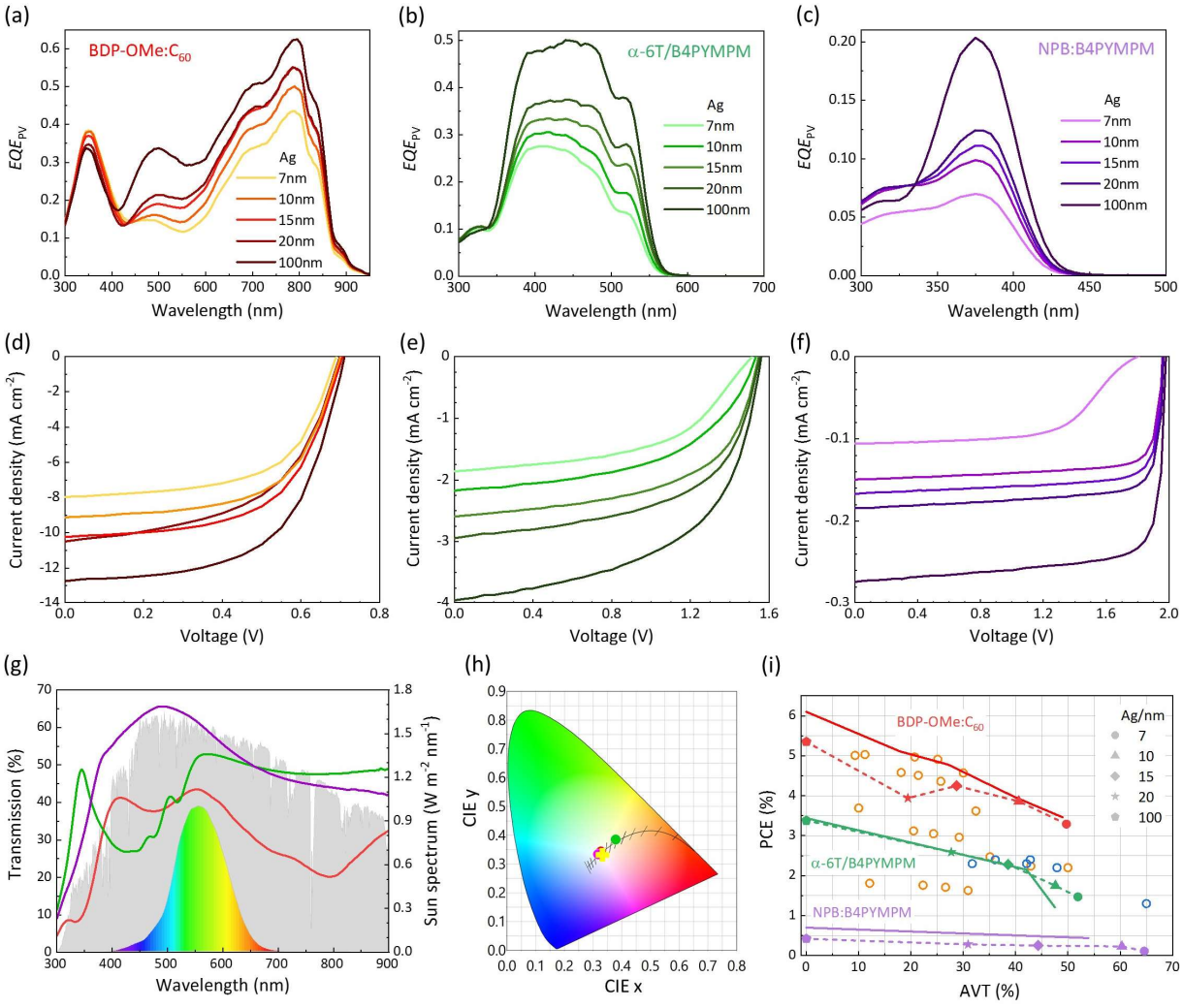


**Fig. 2.** Photovoltaic and optical performance of large-area (2.52 $cm^2$) small-molecular solar cells with varied thickness of Ag. (a, b, c) Photovoltaic external quantum efficiency ($EQE_{PV}$) and (d, e, f) Current density - voltage (*J-V*) characteristics. Pictures of those large-area samples are shown in Figure S5. (g) Transmission spectra for large-area transparent solar cells with 10 nm thick Ag electrodes. The photopic response of the human eye is also shown in rainbow colors. (h) The international commission on illumination CIE 1931 (x, y) coordinates of the transmission spectra for all transparent solar cells with 10 nm thick Ag electrode. Red symbols represent the BDP-OMe:$C_{60}$ combination, green symbols represent α-6T/B4PYMPM devices, and purple symbols represent the NPB:B4PYMPM cells. The yellow cross represents the white light (0.333, 0.333). (i) PCE vs AVT plot for all investigated small-molecule solar cells. Solid lines indicate the performance of devices with a standard active-area of 6.44 $mm^2$, symbol-dash lines represent large-area devices. The reported transparent small-molecule solar cells

processed via solution and thermal evaporation are shown in orange and blue open circles, respectively [20–23].

*3.4 Optical and thermal properties of TSCs*

In addition to the photovoltaic performance, the amount of visible light and solar energy transmitted through the TSC is ascertained by determining their AVT, color rendering index (CRI), and solar heat gain coefficient (SHGC). The reflection and transmission spectra of devices with transparent Ag electrodes are shown in Figure S6, and corresponding values for the AVT, CRI, and SHGC are shown in Table 1. The AVT through the device is calculated based on the transmission $T(\lambda)$ by the following formula [44]:

$$\mathrm{AVT} = \frac{\int_{390}^{830} T(\lambda)P(\lambda)S(\lambda)\mathrm{d}(\lambda)}{\int_{390}^{830} P(\lambda)S(\lambda)\mathrm{d}(\lambda)}, \quad (1)$$

where $\lambda$ is the wavelength and $S(\lambda)$ is the solar spectrum (AM1.5g). The photopic spectral luminous efficiency function $P(\lambda)$ describes the average spectral sensitivity of human vision in regard to brightness [45].

The trends shown in Table 1 make it apparent that reducing the electrode thickness greatly enhances the AVT. With a 10 nm thick Ag electrode, the AVT values for the two UV-absorbing TSCs are excellent: 60.3% for NPB:B4PYMPM, and 47.6% for α-6T/B4PYPMPM. The NIR-absorbing combination BDP-OMe:$C_{60}$ has a decent AVT value of 40%, and has the highest PCE (~ 4%) of the three devices. These BDP-OMe:$C_{60}$ devices show the best efficiency-to-AVT trade-off, with performances that are comparable or superior to previously-reported results in the field of transparent small-molecule solar cells in Fig. 2i [20–23]. Moreover, it has been demonstrated that, when shifting the absorption peaks of molecules from visible to NIR region,

the reduction of PCE in order to get an equivalent AVT (~ 30%) is diminished from 25% to 15% [20]. The main absorption peaks of our devices are not located in the visible region. As a result, this selectively UV/NIR-absorbing property makes the performance reduction of our devices smaller than devices that utilize non-selective absorbers as shown in Figure S7. These results indicate that selectively harvesting sunlight is one way to ameliorate the loss of performance in transparent solar cells.

**Table 1.** Photovoltaic and optical performance of large-area (2.52 $cm^2$) photovoltaic devices.

| | Ag (nm) | $V_{OC}$ (V) | $J_{SC}$ (mA $cm^{-2}$) | *FF* (%) | *PCE* (%) | AVT (%) | CRI | CIE 1931 (x, y) | SHGC |
|---|---|---|---|---|---|---|---|---|---|
| BDP-OMe: $C_{60}$ | 7 | 0.69 | 7.96 | 60.0 | 3.29 | 49.7 | 94 | 0.3398, 0.3505 | 0.46 |
| | 10 | 0.70 | 9.12 | 60.4 | 3.86 | 40.6 | 94 | 0.3274, 0.3430 | 0.37 |
| | 15 | 0.71 | 10.24 | 59.0 | 4.25 | 28.7 | 93 | 0.3112, 0.3303 | 0.28 |
| | 20 | 0.70 | 10.49 | 53.7 | 3.94 | 19.4 | 93 | 0.2974, 0.3171 | 0.22 |
| | 100 | 0.71 | 12.74 | 59.1 | 5.35 | | | | |
| α-6T/ B4PYMPM | 7 | 1.51 | 1.86 | 52.0 | 1.47 | 51.9 | 95 | 0.3766, 0.3812 | 0.56 |
| | 10 | 1.53 | 2.17 | 52.6 | 1.75 | 47.6 | 93 | 0.3793, 0.3852 | 0.48 |
| | 15 | 1.55 | 2.59 | 56.8 | 2.28 | 38.6 | 90 | 0.3624, 0.3788 | 0.31 |
| | 20 | 1.55 | 2.94 | 56.7 | 2.59 | 27.7 | 89 | 0.3515, 0.3729 | 0.24 |
| | 100 | 1.56 | 3.95 | 54.9 | 3.38 | | | | |
| NPB: B4PYMPM | 7 | 1.80 | 0.11 | 59.4 | 0.11 | 64.6 | 98 | 0.3329, 0.3404 | 0.60 |
| | 10 | 1.96 | 0.15 | 77.7 | 0.23 | 60.3 | 99 | 0.3179, 0.3338 | 0.47 |
| | 15 | 1.96 | 0.17 | 77.7 | 0.25 | 44.3 | 98 | 0.2980, 0.3188 | 0.33 |
| | 20 | 1.96 | 0.18 | 77.9 | 0.28 | 30.9 | 98 | 0.2821, 0.3024 | 0.24 |
| | 100 | 1.98 | 0.27 | 77.3 | 0.42 | | | | |

The CRI is a parameter used to quantitatively describe how accurately a light source or transparent medium reproduces the color of a given object, in comparison with the same object illuminated by an ideal light source (e.g. AM 1.5g) [46]. A CRI of 100 would indicate perfect color reproduction. All three of the transparent devices presented here have excellent CRI values, over 93 in the case of devices with 10 nm thick electrodes, indicating remarkable color-rendering qualities. The CIE 1931 (x, y) coordinates of transmission spectra for the transparent

BDP-OMe:$C_{60}$ and NPB:B4PYMPM devices approach those of the solar spectrum as the Ag electrode becomes thinner (Figure S6).

In addition to their optical properties, the amount of solar heat energy our TSCs are able to transmit is also significant for BIPV applications. The SHGC, whose value ranges from 0 to 1, is a parameter that can be used to assess the thermal transfer properties of TSCs [47]. The higher a window's SHGC, the more solar energy it can transmit [48]. The SHGC values for all of our TSCs are strongly correlated with the thickness of the Ag electrode, devices with thinner electrodes have higher SHGC values. The NIR-absorbing BDP-OMe:$C_{60}$ cells are the best at blocking incoming heat, as evidenced by their relatively low SHGC figures compared to the UV-absorbing cells. Its SHGC values are less affected by the reduction in electrode thickness than those for UV-absorbing α-6T/B4PYMPM and NPB:B4PYMPM, which stems from the ability of BDP-OMe:$C_{60}$ to convert more long-wavelength light into electricity than the UV absorbing-devices, thereby reducing the amount of solar energy allowed into the indoor environment. This heat-blocking ability makes BDP-OMe:$C_{60}$-based devices best suited for use in hot climates, as they can help reducing electricity consumption due to air conditioning [49]. The near UV-absorbing solar cells have a lower heat-blocking ability, indicated by their higher SHGCs. These values go up to 60%, which is comparable to a typical double-glazed window (> 60%) [50]. This would make devices based on α-6T/B4PYMPM and NPB:B4PYMPM more appropriate for cooler areas, since they help preserving heat by allowing more NIR light to pass through, thereby keeping the room warm [49].

*3.5 Electrochromic devices*

Organic EC materials have been used in a variety of applications, including self-dimming mirrors and goggles [51], displays [52], and electrochromic e-skins [53]. The organic EC technology described here has distinctive properties, offering a superior on-off contrast ratio along with a low-cost, solution-based fabrication process [30]. Instead of metal oxide layers, the color-switching medium consists of a dye-containing liquid that changes from invisible to black by either electrochemical oxidation or an acid/base reaction [54]. The device itself runs on a low DC voltage that can be provided by the transparent solar cells described in the previous section. The combination of TSCs with ECs offers a promising option for sustainable light and temperature control in residential or office buildings [55].

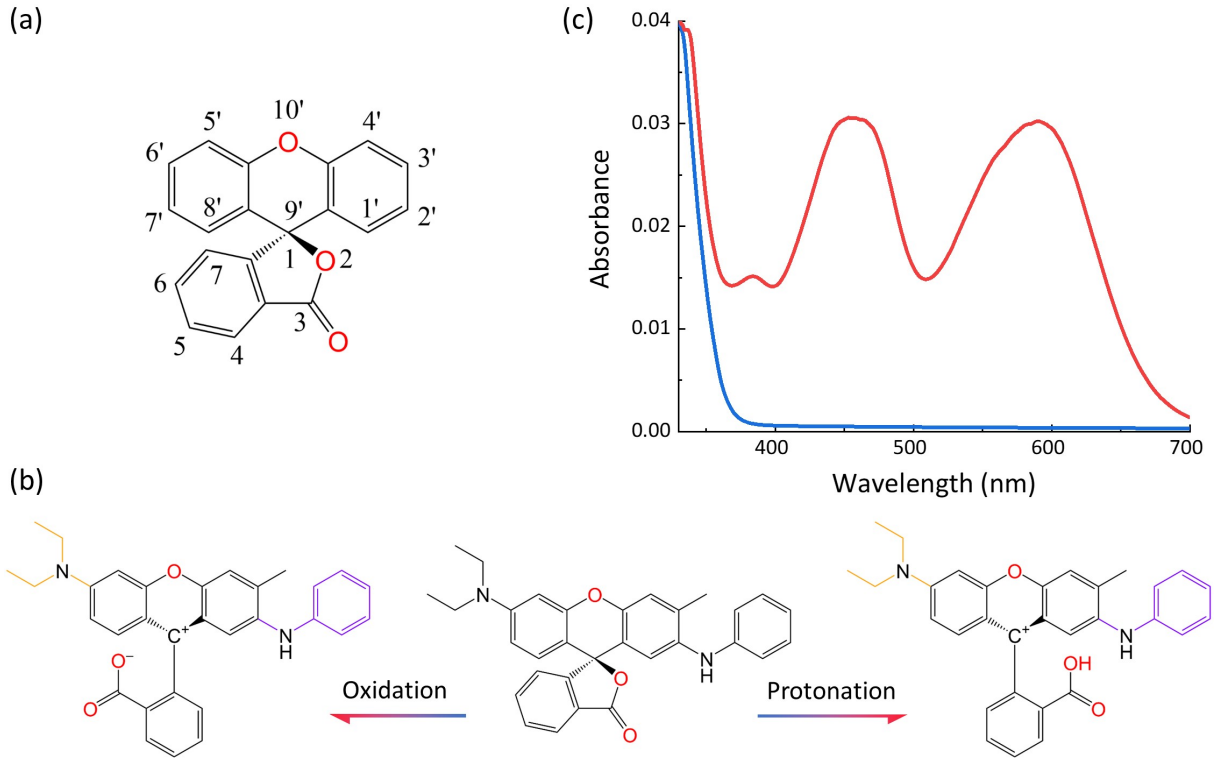


**Fig. 3.** Properties and coloration mechanism of fluoran dye. (a) The core structure of a fluoran dye molecule. (b) The transparent, closed-ring molecule can be switched to black by either oxidation (left) or protonation (right). (c) Absorption spectra of black fluoran dye in its transparent (blue curve) and its darkened states (red curve). The black color stems from the absorption in the whole visible light range, in particular two absorption peaks, one in the violet and one in the yellow region, each of which is associated with separate functional groups

attached to the fluoran dye core. In the case of black fluoran dye, the groups are attached to the 6' and 2' positions [56].

The electrochromic pigment utilized here belongs to the family of fluoran dyes. Fluoran dyes all share the same core molecular structure as shown in Fig. 3a, and the final color is determined by the type and position of functional groups attached to the core [56]. Switching these dyes from transparent to colored is done by cleaving the lactone ring, specifically the bond between 9' and 2 positions. Breaking this bond changes the hybridization of the spiro-carbon from $sp^3$ to $sp^2$, extending the conjugated π-electron system and shifting the HOMO-LUMO level into the visible range [49,57]. This bond-breaking coloration mechanism comes about in our devices via a combination of two different pathways, depicted in Fig. 3b. One is by electrochemical oxidation, wherein coloration occurs upon exposure of the dissolved dye to an electric field [30]. In our devices, this happens by diffusion of the dye molecules to the working electrode. The other coloration pathway is via direct protonation in a Bronsted-Lowry acid/base reaction, where a free $H^+$ ion binds with the oxygen atom in the lactone ring, thereby breaking the C-O bond and extending the molecule's π-conjugation [58,59]. The free $H^+$ ions in our devices come from the oxidation of hydroquinone at the working electrode, which creates benzoquinone and $H^+$ ions. The bleaching of this device occurs by the inverse of the coloration process. Electrochemical reduction and/or deprotonation of the dye molecule closes the lactone ring and resets the dye to its transparent state. Interestingly, this bleaching can happen at either a negative or a neutral bias. The bleaching at 0 V is much slower than at negative bias, because at neutral bias the molecules have to diffuse all the way to the counter-electrode for reduction and deprotonation. At a negative bias, these processes occur directly at the working electrode, so there is no additional wait for diffusion time [30].

A black-hued fluoran dye was chosen for our devices, in part for its excellent optical qualities, and also because it is easily obtained and for example already used ubiquitously in thermal paper (e.g., printed receipts) [56]. The dye's black color stems from the combination of absorption throughout the visible wavelengths in addition to two maxima, found in the yellow and in the violet wavelengths (see Fig. 3c). One maximum occurring around 450 nm is associated with the anilino functional group at the 2' position, and imparts a violet color. The other maximum around 600 nm comes from the alkyl functional group at the 6' position, giving a yellow color. The absorption over the whole visible region, presenting in particular two maxima in the yellow and violet region, results in a black hue.[56,60]

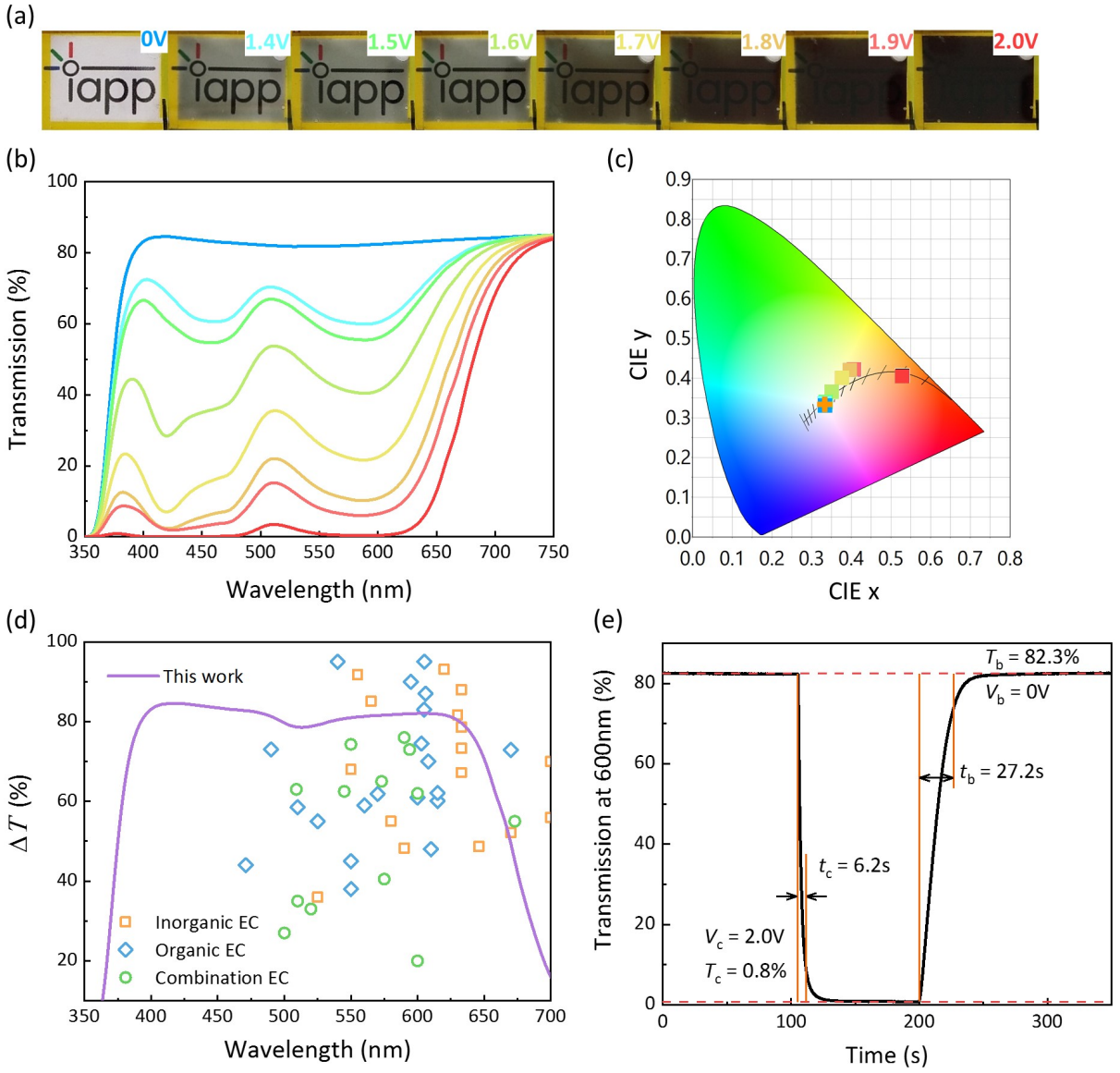


**Fig. 4.** Electrochromic device performances. (a) Photographs and (b) Transmission spectra of a 70 μm-thick EC device held at the same voltage levels as in (a). A Keithley 2602 SMU is used to apply voltages to the EC device and to manipulate its transmission properties. (c) The CIE 1931 (x, y) coordinates of the device in each state when holding voltage changes from 0V to 2V stepwise. Different colors indicate varied turn-on voltages. The coordinate of the solar spectrum as a reference is shown as an orange cross. (d) Comparison of transmission difference ($\Delta T$) between bleached state and darkened state in various types of EC devices. Details can be found in Table S6. (e) Bleaching and coloration times of the EC device extracted for a 90% of transmission change, from which the calculation of the coloration efficiency is shown in Note S2.

Fabrication of an EC device from dihydroxybenzene and fluoran dye involves simply dissolving the components in a solvent along with an electrolyte salt, then sealing the resulting liquid between two sheets of ITO glass. Fig. 4a shows a 70 μm-thick EC device operated by

applying a DC voltage (1.4-2.0 V) to switch the color from clear to deep black, the transmission spectra of which are shown in Fig. 4b. The transmission in the unbiased off-state is very high throughout the visible wavelengths, with an AVT of 82.2%. The fully opaque on-state transmits very little light, with an AVT of 1.7%. Moreover, as shown in Fig. 4d, a high contrast ratio of over 80% can be obtained in the range of 390 to 640 nm, which is comparable or higher than those of commercially available EC smart windows [32]. This EC device can also offer varying shades of black that still allow a portion of visible light to filter through, depending on the initial amount of applied voltage. For a less-intense shade of black, one only needs to use a switching voltage lower than 2 V. A noticeable variance between shades can be seen with about a 0.1 V difference in switching potential. Lighter shades are achieved by applying switching potentials of 1.4-1.6 V, and darker shades come from switching at 1.7-1.9 V. The color quality for each of the states is represented in the CIE (x, y) coordinate plot in Fig. 4c. The EC device in the fully-transparent state has coordinates of (0.333, 0.331), very close to those of the solar spectrum. This indicates that the device in the off-state has a very clear and neutral color quality which is further evidenced by the CRI value of 94 shown in Table S7.

In addition to the contrast ratio between bleached and colored states, switching speed and coloration efficiency are two important metrics to evaluate the performance of EC devices [27]. The switching on and off times for 90% transmission change are extracted, as shown in Fig. 4e. Upon applying a driving voltage of 2.0 V, the EC device needs a coloration time ($t_c$) of 6.2 s to reach a darkened state. However, since no reversed voltage is applied to revert the EC device back to a transparent state, the bleaching time ($t_b$) is longer, 27.2 s. It is worth noticing that a negative bias can indeed speed up the bleaching process: the $t_b$ is decreased to 11.2 s when an

-1 V bias is applied (see Figure S8). The coloration efficiency represents the change in transmission contrast divided by charges consumed per unit of active EC area [7,61]. Compared to inorganic EC devices which have coloration efficiencies in the range of 19 to 133 $cm^2$ $C^{-1}$ [5,7,27], the coloration efficiency of our organic EC device is excellent and can reach up to 147.6 $cm^2$ $C^{-1}$ when its 90% optical density change is achieved. About the stability of our EC devices, several works report that similar fluoran dye based devices exhibit transmittances of bleached and colored states losses below 10% even after 12,000 cycles [30,62,63].

*3.6 Self-powered electrochromic smart window*

We demonstrate now the capability of TSCs to power EC devices in order to manipulate their transmission state. Photographs of EC and EC driven by TSCs are shown in Fig. 5a, and corresponding transmission spectra and calculated optical parameters are shown in Fig. 5b and Table S8. Because its output voltage at the maximum power point is ~ 0.55 V, NIR-absorbing TSCs need to be series-connected to get sufficient voltage to drive the EC device. As shown in Fig. 5a, two series-connected NIR TSCs can only partly dim the EC, while three NIR devices are able to make the transmission change very distinct with AVT and CRI reduced from 82.2% to 19.7% and 93 to 73, respectively. Conversely, NPB-containing TSCs need a parallel connection to produce enough current to make the coloration reaction in the EC device happen. The power density of a single large-area α-6T TSCs under 1 sun intensity is sufficient to drive the EC device because the energy consumption of the EC device is as low as 2.7 W $m^{-2}$ when it is held at 1.6 V as shown in Figure S9. The low energy dissipation of the organic EC makes the self-powered TSC+EC stack possible. The aforementioned stack is made by combining a

2.52 $cm^2$ α-6T containing TSC with a 70 μm-thick EC device with an area of 2.85 $cm^2$. After illumination, the transmission of the organic EC is lowered as shown in Fig. 5d. It is worth to note that the EC can be tuned to a deep darkened state when two series-connected 6T TSCs are employed (see Fig. 5a), which indicates that with the help of well-designed circuit and other electric elements such as resistors, the photovoltaic-powered, transmission-tunable electrochromic window is indeed possible. This self-powered TSC+EC stack has great potential to replace the most common double-glazed windows due to its feasibility in large-scale manufacturing, easy installation, and energy-saving and sunlight-manipulating properties.

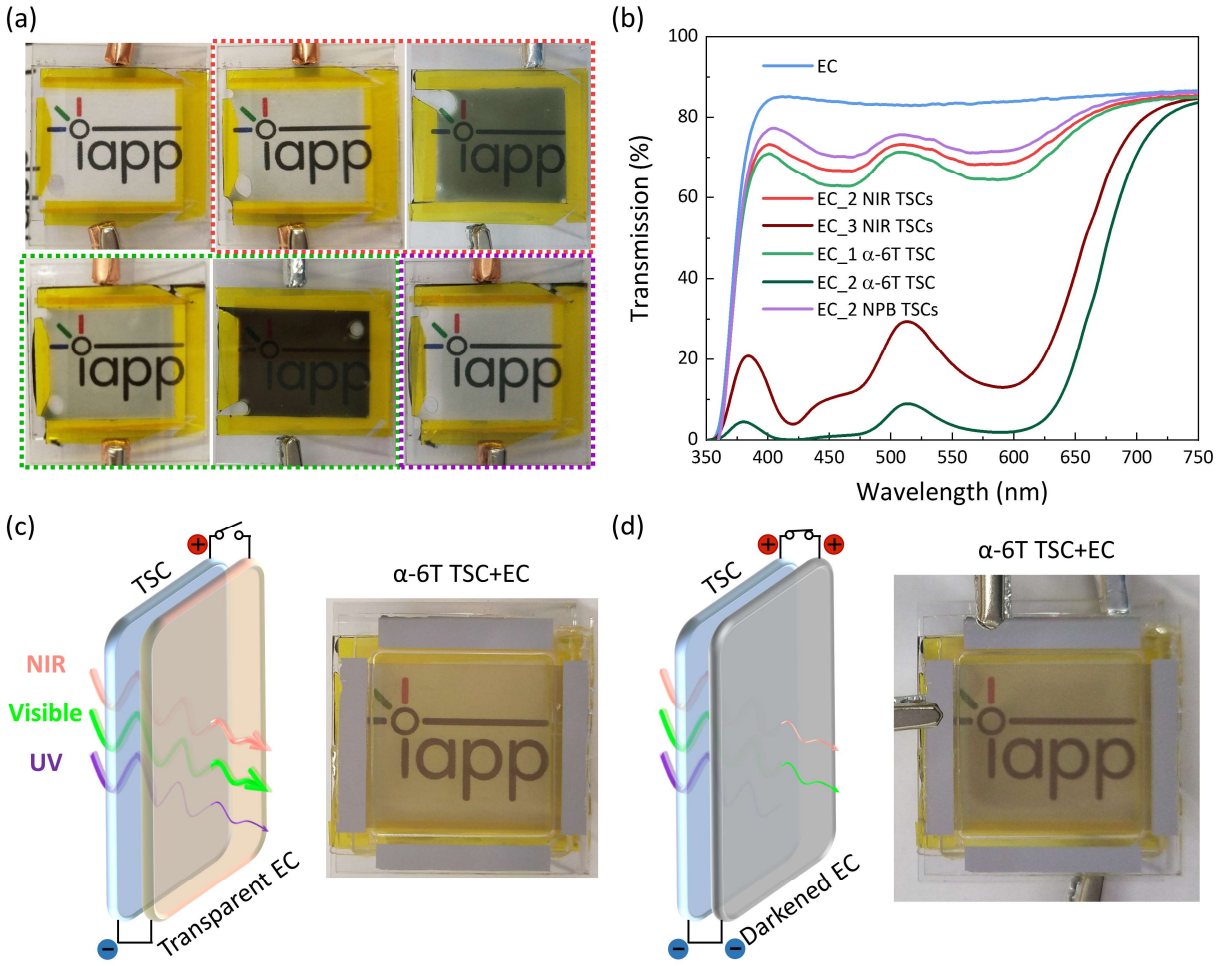


**Fig. 5.** Performance of electrochromic device driven by transparent solar cells. (a) The top left shows an EC device at transparent state, the top right shows the EC powered by two or three series-connected BDP-OMe:$C_{60}$ NIR TSCs respectively (red box) as demonstrated in Figure S10. The EC charged by one or two α-6T/B4PYMPM TSCs are shown on the bottom left in a

green box and on the bottom right by two parallel-connected NPB:B4PYMPM TSCs, shown in a purple box. The illumination intensity for all the TSCs is ~1 sun. (b) Corresponding transmission spectra of the EC device manipulated by TSCs. (c) Schematic illustration of electrochromic smart window connected with transparent solar cells as a promising alternative to traditional double-glazed windows. The front view of the real stack of α-6T/B4PYMPM and EC is shown on the right. (d) Schematic illustration and real self-powered TSC+EC stack at the darkened state.

## 4. Conclusion

We have demonstrated a promising combination of transparent large-area (2.52 $cm^2$) small-molecule solar cells with a low-cost, solution-processed organic electrochromic device. Our UV-TSCs exhibit ample AVT and excellent color quality as well as high photovoltage (>1.5 V). The NIR-harvesting blend BDP-OMe:$C_{60}$ shows a PCE of ~ 4% with an AVT of ~ 40%, which are superior compared with reported small molecule based TSCs. UV/NIR TSCs in series or parallel connection are able to drive fluoran-based EC devices and to manipulate its AVT from 82.2% to 1.7%. Our results show that UV/NIR selectively absorbing TSCs are good candidates for power-generating windows without sacrificing the transmission of visible light. The EC device's remarkable on/off contrast ratio and adjustable transmission properties make these suitable for controlling the indoor climate, which is important to realize smart energy-efficient buildings. We hope this work will inspire more efforts into the synthesis of high-efficiency, selectively absorbing, PV materials, and more advanced techniques to enlarge the area of TSCs over 1 $m^2$ without significant performance reduction.

## Acknowledgments

X.J. thanks support from the China Scholarship Council (no. 201706140127) and Graduate Academy of Technische Universität Dresden. The authors acknowledge the Free State of Saxony and the European Regional Development Fund for financial support within the project REAL (100364085).

## Author contributions

X.J., D.S., and K.V. designed the experiments, prepared photovoltaic devices, and optimized their performance. X.J. performed the J-V and EQE measurements for all solar cells. E.C.B. and X.J. prepared electrochromic devices and performed UV-Vis measurements for EC devices; X.J. did this measurement for transparent solar cells. J.B-N., S.R., K.V., and D.S. supervised their team members involved in this project. X.J. and E.C.B. wrote the manuscript. All authors contributed to the critical analysis of the findings and the revision of the manuscript. D.S supervised the overall project.

## Competing interests

The authors declare no competing interests.

## References


[1] A. Ghosh, B. Norton, Advances in switchable and highly insulating autonomous (self-powered) glazing systems for adaptive low energy buildings, Renew. Energy. 126 (2018) 1003–1031. https://doi.org/10.1016/j.renene.2018.04.038.

[2] A. Detollenaere - Becquerel Institute, Snapshot of Global PV Markets 2020 PVPS Task 1 Strategic PV Analysis and Outreach, 2020. www.iea-pvps.org (accessed September 2, 2020).

[3] B.P. Jelle, Building integrated photovoltaics: A concise description of the current state of the art and possible research pathways, Energies. 9 (2016) 1–30. https://doi.org/10.3390/en9010021.

[4] A. Cannavale, F. Martellotta, F. Fiorito, U. Ayr, The Challenge for Building Integration of Highly Transparent Photovoltaics and Photoelectrochromic Devices, Energies. 13 (2020) 1929. https://doi.org/10.3390/en13081929.

[5] C.J. Barile, D.J. Slotcavage, J. Hou, M.T. Strand, T.S. Hernandez, M.D. McGehee, Dynamic Windows with Neutral Color, High Contrast, and Excellent Durability Using Reversible Metal Electrodeposition, Joule. 1 (2017) 133–145. https://doi.org/10.1016/j.joule.2017.06.001.

[6] X.H. Li, C. Liu, S.P. Feng, N.X. Fang, Broadband Light Management with Thermochromic Hydrogel Microparticles for Smart Windows, Joule. 3 (2019) 290–302. https://doi.org/10.1016/j.joule.2018.10.019.

[7] H. Fang, P. Zheng, R. Ma, C. Xu, G. Yang, Q. Wang, H. Wang, Multifunctional hydrogel enables extremely simplified electrochromic devices for smart windows and ionic writing boards, Mater. Horizons. 5 (2018) 1000–1007. https://doi.org/10.1039/c8mh00856f.

[8] K. Lee, H. Um, D. Choi, J. Park, N. Kim, H. Kim, K. Seo, The Development of Transparent Photovoltaics, Cell Reports Phys. Sci. 1 (2020) 100143. https://doi.org/10.1016/j.xcrp.2020.100143.

[9] Y. Cui, C. Yang, H. Yao, J. Zhu, Y. Wang, G. Jia, F. Gao, J. Hou, Efficient Semitransparent Organic Solar Cells with Tunable Color enabled by an Ultralow-Bandgap Nonfullerene Acceptor, Adv. Mater. 29 (2017) 1–7. https://doi.org/10.1002/adma.201703080.

[10] W. Wang, C. Yan, T.-K. Lau, J. Wang, K. Liu, Y. Fan, X. Lu, X. Zhan, Fused Hexacyclic Nonfullerene Acceptor with Strong Near-Infrared Absorption for Semitransparent Organic Solar Cells with 9.77% Efficiency, Adv. Mater. 29 (2017) 1701308.

https://doi.org/10.1002/adma.201701308.

[11] B. Jia, S. Dai, Z. Ke, C. Yan, W. Ma, X. Zhan, Breaking 10% Efficiency in Semitransparent Solar Cells with Fused-Undecacyclic Electron Acceptor, Chem. Mater. 30 (2018) 239–245. https://doi.org/10.1021/acs.chemmater.7b04251.

[12] H. Chen, H. Lai, Z. Chen, Y. Zhu, H. Wang, L. Han, Y. Zhang, F. He, 17.1 %-Efficient Eco-Compatible Organic Solar Cells from a Dissymmetric 3D Network Acceptor, Angew. Chemie. 132 (2020) 2–11. https://doi.org/10.1002/ange.202013053.

[13] G.P. Kini, S.J. Jeon, D.K. Moon, Latest Progress on Photoabsorbent Materials for Multifunctional Semitransparent Organic Solar Cells, Adv. Funct. Mater. 2007931 (2021) 2007931. https://doi.org/10.1002/adfm.202007931.

[14] Z. Hu, J. Wang, X. Ma, J. Gao, C. Xu, K. Yang, Z. Wang, J. Zhang, F. Zhang, A critical review on semitransparent organic solar cells, Nano Energy. 78 (2020) 105376. https://doi.org/10.1016/j.nanoen.2020.105376.

[15] X. Li, H. Meng, F. Shen, D. Su, S. Huo, J. Shan, J. Huang, C. Zhan, Semitransparent fullerene-free polymer solar cell with 44% AVT and 7% efficiency based on a new chlorinated small molecule acceptor, Dye. Pigment. 166 (2019) 196–202. https://doi.org/10.1016/j.dyepig.2019.03.024.

[16] W. Su, Q. Fan, X. Guo, J. Wu, M. Zhang, Y. Li, Efficient as-cast semi-transparent organic solar cells with efficiency over 9% and a high average visible transmittance of 27.6%, Phys. Chem. Chem. Phys. 21 (2019) 10660–10666. https://doi.org/10.1039/C9CP01101C.

[17] E. Pascual-San-José, G. Sadoughi, L. Lucera, M. Stella, E. Martínez-Ferrero, G.E. Morse, M. Campoy-Quiles, I. Burgués-Ceballos, Towards photovoltaic windows: scalable fabrication of semitransparent modules based on non-fullerene acceptors via laser-patterning, J. Mater. Chem. A. 8 (2020) 9882–9895. https://doi.org/10.1039/D0TA02994G.

[18] J. Zhang, G. Xu, F. Tao, G. Zeng, M. Zhang, Y. (Michael) Yang, Y. Li, Y. Li, Highly Efficient Semitransparent Organic Solar Cells with Color Rendering Index Approaching 100, Adv. Mater. 31 (2019) 1807159. https://doi.org/10.1002/adma.201807159.

[19] M. Riede, D. Spoltore, K. Leo, Organic Solar Cells—The Path to Commercial Success, Adv. Energy Mater. 2002653 (2020) 1–10. https://doi.org/10.1002/aenm.202002653.

[20] D. Yang, T. Sano, H. Sasabe, L. Yang, S. Ohisa, Y. Chen, Y. Huang, J. Kido, Colorful Squaraines

Dyes for Efficient Solution-Processed All Small-Molecule Semitransparent Organic Solar Cells, ACS Appl. Mater. Interfaces. 10 (2018) 26465–26472. https://doi.org/10.1021/acsami.8b08878.

[21] J. Min, C. Bronnbauer, Z.G. Zhang, C. Cui, Y.N. Luponosov, I. Ata, P. Schweizer, T. Przybilla, F. Guo, T. Ameri, K. Forberich, E. Spiecker, P. Bäuerle, S.A. Ponomarenko, Y. Li, C.J. Brabec, Fully Solution-Processed Small Molecule Semitransparent Solar Cells: Optimization of Transparent Cathode Architecture and Four Absorbing Layers, Adv. Funct. Mater. 26 (2016) 4543–4550. https://doi.org/10.1002/adfm.201505411.

[22] R.R. Lunt, V. Bulovic, Transparent, near-infrared organic photovoltaic solar cells for window and energy-scavenging applications, Appl. Phys. Lett. 98 (2011) 113305. https://doi.org/10.1063/1.3567516.

[23] J. Meiss, F. Holzmueller, R. Gresser, K. Leo, M. Riede, Near-infrared absorbing semitransparent organic solar cells, Appl. Phys. Lett. 99 (2011) 193307. https://doi.org/10.1063/1.3660708.

[24] N. DeForest, A. Shehabi, S. Selkowitz, D.J. Milliron, A comparative energy analysis of three electrochromic glazing technologies in commercial and residential buildings, Appl. Energy. 192 (2017) 95–109. https://doi.org/10.1016/j.apenergy.2017.02.007.

[25] S.-I. Park, Y.-J. Quan, S.-H.S. Kim, H. Kim, S.-H.S. Kim, D.-M. Chun, C.S. Lee, M. Taya, W.-S. Chu, S.-H. Ahn, A review on fabrication processes for electrochromic devices, Int. J. Precis. Eng. Manuf. Technol. 3 (2016) 397–421. https://doi.org/10.1007/s40684-016-0049-8.

[26] X. Xia, Z. Ku, D. Zhou, Y. Zhong, Y. Zhang, Y. Wang, M.J. Huang, J. Tu, H.J. Fan, Perovskite solar cell powered electrochromic batteries for smart windows, Mater. Horizons. 3 (2016) 588–595. https://doi.org/10.1039/C6MH00159A.

[27] Y. Ke, J. Chen, G. Lin, S. Wang, Y. Zhou, J. Yin, P.S. Lee, Y. Long, Smart Windows: Electro-, Thermo-, Mechano-, Photochromics, and Beyond, Adv. Energy Mater. 9 (2019) 1902066. https://doi.org/10.1002/aenm.201902066.

[28] K. Kanazawa, K. Nakamura, N. Kobayashi, Electroswitchable optical device enabling both luminescence and coloration control consisted of fluoran dye and 1,4-benzoquinone, Sol. Energy Mater. Sol. Cells. 145 (2016) 42–53. https://doi.org/10.1016/j.solmat.2015.06.061.

[29] I.J. Ko, J.H. Park, G.W. Kim, R. Lampande, J.H. Kwon, An optically efficient full-color reflective display with an electrochromic device and color production units, J. Inf. Disp. 20 (2019) 155–160. https://doi.org/10.1080/15980316.2019.1649310.

[30] G.W. Kim, Y.C. Kim, I.J. Ko, J.H. Park, H.W. Bae, R. Lampande, J.H. Kwon, High-Performance Electrochromic Optical Shutter Based on Fluoran Dye for Visibility Enhancement of Augmented Reality Display, Adv. Opt. Mater. 6 (2018) 1701382. https://doi.org/10.1002/adom.201701382.

[31] D.C. Choe, G.W. Kim, R. Lampande, J.H. Kwon, 54.4: Smart Window Devices for Black Screen of Organic Light Emitting Diodes, SID Symp. Dig. Tech. Pap. 46 (2015) 821–823. https://doi.org/10.1002/sdtp.10343.

[32] M. Casini, Active dynamic windows for buildings: A review, Renew. Energy. 119 (2018) 923–934. https://doi.org/10.1016/j.renene.2017.12.049.

[33] J. Feng, F. Li, W. Gao, S. Liu, Y. Liu, Y. Wang, White light emission from exciplex using tris-(8-hydroxyquinoline)aluminum as chromaticity-tuning layer, Appl. Phys. Lett. 78 (2001) 3947–3949. https://doi.org/10.1063/1.1379788.

[34] V.C. Nikolis, J. Benduhn, F. Holzmueller, F. Piersimoni, M. Lau, O. Zeika, D. Neher, C. Koerner, D. Spoltore, K. Vandewal, Reducing Voltage Losses in Cascade Organic Solar Cells while Maintaining High External Quantum Efficiencies, Adv. Energy Mater. 7 (2017) 1700855. https://doi.org/10.1002/aenm.201700855.

[35] S. Ullbrich, J. Benduhn, X. Jia, V.C.V.C. Nikolis, K. Tvingstedt, F. Piersimoni, S. Roland, Y. Liu, J. Wu, A. Fischer, D. Neher, S. Reineke, D. Spoltore, K. Vandewal, Emissive and charge-generating donor–acceptor interfaces for organic optoelectronics with low voltage losses, Nat. Mater. 18 (2019) 459–464. https://doi.org/10.1038/s41563-019-0324-5.

[36] H. Sasabe, D. Tanaka, D. Yokoyama, T. Chiba, Y.-J. Pu, K. Nakayama, M. Yokoyama, J. Kido, Influence of Substituted Pyridine Rings on Physical Properties and Electron Mobilities of 2-Methylpyrimidine Skeleton-Based Electron Transporters, Adv. Funct. Mater. 21 (2011) 336–342. https://doi.org/10.1002/adfm.201001252.

[37] W. Zhao, A. Kahn, Charge transfer at n-doped organic-organic heterojunctions, J. Appl. Phys. 105 (2009) 123711. https://doi.org/10.1063/1.3153962.

[38] Fraunhofer FEP and Heliatek: Conclusion of BMBF research project on transparent organic photovoltaic glass façades (TOP) - OPE Journal - Organic & Printed Electronics, (n.d.). https://ope-journal.com/news/fraunhofer-fep-and-heliatek-conclusion-of-bmbf-research-project-on-transparent-organic-photovoltaic-glass-facades-top (accessed May 21, 2021).

[39] Q. Burlingame, X. Huang, X. Liu, C. Jeong, C. Coburn, S.R. Forrest, Intrinsically stable organic

546 solar cells under high-intensity illumination, Nature. 573 (2019) 394–397.
547 https://doi.org/10.1038/s41586-019-1544-1.
548 [40] S. Ben Dkhil, M. Pfannmöller, S. Bals, T. Koganezawa, N. Yoshimoto, D. Hannani, M. Gaceur,
549 C. Videlot-Ackermann, O. Margeat, J. Ackermann, Square-Centimeter-Sized High-Efficiency
550 Polymer Solar Cells: How the Processing Atmosphere and Film Quality Influence Performance
551 at Large Scale, Adv. Energy Mater. 6 (2016) 1600290. https://doi.org/10.1002/aenm.201600290.
552 [41] S. Lenk, T. Schwab, S. Schubert, L. Müller-Meskamp, K. Leo, M.C. Gather, S. Reineke, White
553 organic light-emitting diodes with 4 nm metal electrode, Appl. Phys. Lett. 107 (2015) 163302.
554 https://doi.org/10.1063/1.4934274.
555 [42] X. Xiao, K. Lee, S.R. Forrest, Inverted, semitransparent small molecule photovoltaic cells, Appl.
556 Phys. Lett. 107 (2015) 033901. https://doi.org/10.1063/1.4927142.
557 [43] R.J. Peh, Y. Lu, F. Zhao, C.-L.K. Lee, W.L. Kwan, Vacuum-free processed transparent inverted
558 organic solar cells with spray-coated PEDOT:PSS anode, Sol. Energy Mater. Sol. Cells. 95 (2011)
559 3579–3584. https://doi.org/10.1016/j.solmat.2011.09.018.
560 [44] C.J. Traverse, R. Pandey, M.C. Barr, R.R. Lunt, Emergence of highly transparent photovoltaics
561 for distributed applications, Nat. Energy. 2 (2017) 849–860. https://doi.org/10.1038/s41560-017-
562 0016-9.
563 [45] L.T. Sharpe, A. Stockman, W. Jagla, H. Jägle, A luminous efficiency function, VD65* (λ), for
564 daylight adaptation: A correction, Color Res. Appl. 36 (2011) 42–46.
565 https://doi.org/10.1002/col.20602.
566 [46] J. Hye Oh, S. Ji Yang, Y. Rag Do, Healthy, natural, efficient and tunable lighting: four-package
567 white LEDs for optimizing the circadian effect, color quality and vision performance, Light Sci.
568 Appl. 3 (2014) e141–e141. https://doi.org/10.1038/lsa.2014.22.
569 [47] University of Minnesota, Windows for High-performance Commercial Buildings,
570 Commercialwindows.Org. (2011) 1–3. https://www.commercialwindows.org/shgc.php
571 (accessed September 9, 2020).
572 [48] Window Selection Tool | Efficient Windows Collaborative, (n.d.).
573 https://www.efficientwindows.org/new-selection1/ (accessed November 13, 2020).
574 [49] A. Piccolo, F. Simone, Performance requirements for electrochromic smart window, J. Build.
575 Eng. 3 (2015) 94–103. https://doi.org/10.1016/j.jobe.2015.07.002.

[50] Window Technologies: Glazing Types - Double Low-E Glazing - Efficient Windows, (n.d.). https://www.efficientwindows.org/gtypes-2lowe/ (accessed November 13, 2020).

[51] C.-G. Granqvist, Out of a niche, Nat. Mater. 5 (2006) 89–90. https://doi.org/10.1038/nmat1577.

[52] M. Grätzel, Ultrafast colour displays, Nature. 409 (2001) 575–576. https://doi.org/10.1038/35054655.

[53] H.-H. Chou, A. Nguyen, A. Chortos, J.W. To, C. Lu, J. Mei, T. Kurosawa, W.-G. Bae, J.B.-H. Tok, Z. Bao, A chameleon-inspired stretchable electronic skin with interactive colour changing controlled by tactile sensing, Nat. Commun. 6 (2015) 8011. https://doi.org/10.1038/ncomms9011.

[54] J.H.. Kwon, D.C. Choe, Smart window comprising electrochromic device and organic light-emitting device, US 9,711,571 B2, 2017.

[55] A.L. Dyer, R.H. Bulloch, Y. Zhou, B. Kippelen, J.R. Reynolds, F. Zhang, A Vertically Integrated Solar-Powered Electrochromic Window for Energy Efficient Buildings, Adv. Mater. 26 (2014) 4895–4900. https://doi.org/10.1002/adma.201401400.

[56] Y. Takahashi, A. Shirai, T. Segawa, T. Takahashi, K. Sakakibara, Why Does a Color-Developing Phenomenon Occur on Thermal Paper Comprising of a Fluoran Dye and a Color Developer Molecule?, Bull. Chem. Soc. Jpn. 75 (2002) 2225–2231. https://doi.org/10.1246/bcsj.75.2225.

[57] G.W. Kim, R. Lampande, D.C. Choe, I.J. Ko, J.H. Park, R. Pode, J.H. Kwon, Next generation smart window display using transparent organic display and light blocking screen, Opt. Express. 26 (2018) 8493. https://doi.org/10.1364/OE.26.008493.

[58] R. Muthyala, Chemistry and Applications of Leuco Dyes, Springer US, Boston, MA, 2002. https://doi.org/10.1007/b114004.

[59] M. Yanagita, I. Aoki, S. Tokita, 13 C NMR and Electronic Absorption Spectroscopic Studies on the Equilibrium between the Colorless Lactone and the Colored Zwitterion Forms of a Fluoran-Based Black Color Former, Bull. Chem. Soc. Jpn. 70 (1997) 2757–2763. https://doi.org/10.1246/bcsj.70.2757.

[60] M. Hojo, T. Ueda, M. Yamasaki, A. Inoue, S. Tokita, M. Yanagita, 1 H and 13 C NMR Detection of the Carbocations or Zwitterions from Rhodamine B Base, a Fluoran-Based Black Color Former, Trityl Benzoate, and Methoxy-Substituted Trityl Chlorides in the Presence of Alkali Metal or Alkaline Earth Metal Perchlorates in Acet, Bull. Chem. Soc. Jpn. 75 (2002) 1569–1576. https://doi.org/10.1246/bcsj.75.1569.

[61] G. Cai, X. Cheng, M. Layani, A.W.M. Tan, S. Li, A.L.-S. Eh, D. Gao, S. Magdassi, P.S. Lee, Direct inkjet-patterning of energy efficient flexible electrochromics, Nano Energy. 49 (2018) 147–154. https://doi.org/10.1016/j.nanoen.2018.04.017.

[62] Y. Wang, S. Wang, X. Wang, W. Zhang, W. Zheng, Y.-M. Zhang, S.X.-A. Zhang, A multicolour bistable electronic shelf label based on intramolecular proton-coupled electron transfer, Nat. Mater. 18 (2019) 1335–1342. https://doi.org/10.1038/s41563-019-0471-8.

[63] W. Weng, T. Higuchi, M. Suzuki, T. Fukuoka, T. Shimomura, M. Ono, L. Radhakrishnan, H. Wang, N. Suzuki, H. Oveisi, Y. Yamauchi, A High-Speed Passive-Matrix Electrochromic Display Using a Mesoporous TiO2 Electrode with Vertical Porosity, Angew. Chemie. 122 (2010) 4048–4051. https://doi.org/10.1002/ange.200907008.

618 TOC Graphic:

619 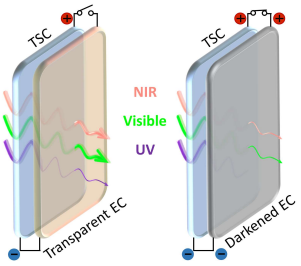


620

## Highlights

- A prototype of a self-powered electrochromic smart window is demonstrated, which can dynamically modulate the sunlight transmission.
- Selectively UV-harvesting transparent solar cells (TSCs) show respectable average visible-light transmission (AVT, ~ 50-65%) and offer high photovoltages (1.5-2.0 V) to drive electrochromic devices.
- NIR-absorbing TSCs with an area of 2.52 $cm^2$ exhibit an efficiency of ~ 4% and an AVT of ~ 40%, which is the highest performance among reported small-molecule-based TSCs.
- High contrast ratio of electrochromic device over 80% in the range of 390 to 640 nm.